Ivanova, A., Kashubin, A., Juhojuntti, N., Kummerow, J., Henninges, J., Juhlin, C., Lüth, S., Ivandic, M. (2012): Monitoring and volumetric estimation of injected CO2 using 4D seismic, petrophysical data, core measurements and well logging: a case study at Ketzin, Germany. - Geophysical Prospecting, 60, 5, 957-973

DOI: 10.1111/j.1365-2478.2012.01045.x

Monitoring and volumetric estimation of injected CO_2 using 4D seismic, petrophysical data, core measurements and well logging: a case study at Ketzin, Germany

Alexandra Ivanova[1, 2*], Artem Kashubin[2], Niklas Juhojuntti[2], Juliane Kummerow[1], Jan Henninges[1], Christopher Juhlin[2], Stefan Lüth[1], Monika Ivandic[2]

[1]Helmholtz-Zentrum Potsdam Deutsches GeoForschungsZentrum (GFZ), Centre for CO_2-Storage, Telegrafenberg, 14473, Potsdam, Germany

[2]Department of Earth Sciences, Uppsala University, Uppsala 75236, Sweden

(E-mail: aivanova@gfz-potsdam.de / Fax: +49 331-2881502 / Phone: +49 331-2881972)

ABSTRACT

More than 50000 tons of CO_2 have been injected at Ketzin into the Stuttgart Formation, a saline aquifer, at approximately 620 m depth, as of the summer 2011. We present here results from the 1st repeat 3D seismic survey that was performed at the site in the autumn 2009, after about 22000 tons of CO_2 had been injected. We show here that rather complex time-lapse signatures of this CO_2 can be clearly observed within a radius of about 300 m from the injection well. The highly irregular amplitude response within this radius is attributed to the heterogeneity of the injection reservoir. Time delays to a reflection below the injection level are also observed. Petrophysical measurements on core samples and geophysical logging of CO_2 saturation levels allow an estimate of the total amount of CO_2 visible in the seismic data to be made. These estimates are somewhat lower than the actual amount of CO_2 injected at the time of the survey and they are dependent upon the choice of a number of parameters. In spite of some uncertainty, the close agreement between the amount injected and the amount observed is encouraging for quantitative monitoring of CO_2 storage site using seismic methods.

Keywords: Data processing; Monitoring; Rock Physics; Seismics; Time lapse

INTRODUCTION

Capture and geological storage of carbon dioxide (CCS) is an important option to reduce greenhouse gas emissions into the atmosphere (Bachu 2003, IPCC 2005). At Ketzin (Germany), a town close to Berlin, the first European onshore pilot scale project was initiated in 2004 (Schilling *et al.* 2009; Würdemann *et al*. 2010). After baseline characterization, surveying and drilling, CO_2 injection started in June 2008. The injection site is located on a flank of an anticlinal structure (Fig. 1). Small amounts of CO_2 have been injected there (as of June 2011, ~50 kilotons) in comparison to large scale CCS projects, such as, e.g. the Sleipner field (Arts *et al.* 2004) and the In Salah project (Ringrose *et al.* 2009). CO_2 is injected in a super-critical state into sandstones of the Stuttgart Formation, a saline aquifer, at 620-650 m depth, but it is not in a super-critical state within the reservoir as it is in the Sleipner field. The focus of the Ketzin project is on testing and further developing monitoring technologies for CO_2 storage like in other small-scale CCS projects (e.g.Kikuta *et al.* 2004; Michel *et al.* 2010). It consists of geophysical, geochemical, and microbial investigations (Giese *et al.* 2009).

3D seismic time-lapse surveys ("4D seismics") are an essential tool for large scale reservoir characterization and for providing information on injection related processes (e.g. Lumley *et al.* 2003; Gonzalez-Carballo *et al.* 2006), including geological storage of CO_2 (Meadows 2008). This method has proven to be a suitable technique for monitoring CO_2 injected into saline aquifers (Eiken *et al.* 2000) demonstrating time-lapse changes in terms of reflection amplitudes and time delays of reflections from below the injection horizon (the amplitude tuning effect and the velocity push-down effect).

At Ketzin, a 3D baseline seismic survey was acquired in autumn 2005. It revealed a sequence of clear reflections from approximately 150 ms down to 900 ms t.w.t. in a stacked volume (Juhlin *et al.* 2007). After three wells (one injection well and two observation wells) were drilled at the site down to about 800 m in 2007 (Prevedel *et al.* 2008) and CO_2 injection started in June 2008, a smaller 3D seismic repeat survey was acquired in the autumn of 2009 in the area around the injection site. The outlines of the two surveys are shown in Fig. 1. In 2012 a 3D survey is to be repeated again. The last time-lapse seismic survey acquired in Ketzin was performed in February 2011 on seven lines (2D) being simultaneously used as a fixed spread. It was the 2nd repeat using seven 2D lines as a fixed spread. The 1st repeat with this 2D geometry showed no time-lapse anomaly along the 2D lines (Bergmann *et al.* 2011).

In this contribution, we present the processing results for the first repeat 3D measurements, and perform a comparison of the repeat data with the baseline survey. Petrophysical investigations on the reservoir rocks are discussed with regard to the Gassmann theory of effective properties and the patchy saturation models. Results from pulsed neutron-gamma (PNG) logging measurements are shown regarding the CO_2 saturation in the reservoir. Finally, an approach is described, to quantify the amount of CO_2 as imaged by the seismic measurements using petrophysical models and results from PNG logging. This estimate can be used as a base for assessing the ability of repeat 3D seismic surveys to quantify the amount of CO_2 present in a storage reservoir.

GEOLOGICAL SETTING

Fig. 1 shows the depth contour of the top of the Triassic Stuttgart Formation forming a gently dipping anticline close to Ketzin. The anticline is the result of a salt pillow intrusion at a present-day depth of 1500 – 2000 m (Förster *et al.* 2009). The CO_2 is injected into the

sandstones of the Stuttgart Formation at 620 – 650 m depth. The top seal of the Stuttgart Formation is the Triassic Weser Formation. Above these units, several aquifers and aquitards are present, forming a multi-barrier system for the storage horizon (Fig. 2).

Compared to previous 2D vintage seismic data, the 3D baseline survey reveals in greater detail a fault system across the top of the anticline, termed the Central Graben Fault Zone (Juhlin *et al.* 2007). The faults are well developed in the Jurassic section and some possibly extend down to the level of the Stuttgart Formation (Förster *et al.* 2009).

Lithologically, the Stuttgart Formation is characterized by alternating sandy channel-(string)-facies, levee and crevasse-splay deposits, and muddy flood-plain facies rocks. This conbination results in an extremely heterogeneous porosity and permeability distribution. Evidence for significant lateral heterogeneity in the Stuttgart Formation is also found in the amplitude analysis of the 3D baseline seismic data (Kazemeini *et al.* 2009). The top seal formation (Weser) mostly consists of mudstone, clayey siltstone, and anhydrite. The Top of the Weser Formation is marked by a ~20 m thick anhydrite layer which appears as a strong and persistent reflecting horizon in the seismic data throughout the survey area ("K2") (Fig. 2).

DATA ACQUISITION

Acquisition was carried out using the acquisition parameters and a template scheme identical to the acquisition parameters and the template scheme used for the 2005 baseline survey (Table 1, Fig. 3), (Juhlin *et al.* 2007), but with using only 20 templates out of the original 41 templates of the full baseline survey. As in the baseline survey, the nominal fold of 25 was not reached for all CDP bins of the survey area due to logistical constraints from roads, villages

and infrastructure, particularly close to the injection site (Fig. 4). The repeat measurements were carried out under rainy weather conditions that resulted in partly wet, and in some areas inaccessible, fields. These conditions restricted source access to an area at the southern margin of the survey and left a gap in the coverage there (Fig. 4). Apart from this, the baseline acquisition geometry was reproduced at high precision. Only ~1.7% of the receiver positions differed by more than 0.5 m, and only ~3.4% of the source positions differed by more than 0.5 m horizontally. Vertical differences by more than 0.5 m were observed for only two receiver and eight source positions, respectively.

Acquisition lasted from the 25th of September through the 6th of November. About 3250 source points were activated using an accelerated weight drop source during 34 days of active acquisition.

Table 1: Acquisition parameters overview.

Parameter	***Value***
Receiver line spacing / number	96 m / 5
Receiver station spacing / channels	24 m /48
Source line spacing / number	48 m / 12
Source point spacing	24 m or 72 m
CDP bin size	12 m x 12 m
Nominal fold	25
Geophones	28 Hz single
Sampling rate	1 ms
Record length	3 s

Source	240 kg accelerated weight drop, 8 hits per source point
Acquisition unit	Sercel 408 UL

DATA PROCESSING

Data from the baseline and repeat surveys were limited to subsets where only traces that were common for both surveys were included in the processing in order to maximize repeatability in fold and azimuthal coverage. Processing of the repeat seismic data followed the same steps as the baseline data processing (described by Juhlin *et al.* (2007)). New coordinates of the source and receiver locations were re-surveyed for the repeat measurements. They were checked for consistency and loaded into the trace headers in the pre-processing stage. Even though the repeat 3D data were acquired over a smaller area, the same CDP grid of inlines and crosslines covering the entire area was used. Analysis of the raw data showed that the energy content in the higher frequencies of the repeat dataset appeared to be lower for some parts of the area in comparison to the baseline. The baseline and the repeat data were, therefore, reprocessed with a more limited frequency band for easier calibration and further analysis of the time-lapse difference. The processing steps with the original parameters (from Juhlin *et al.* (2007)) and the new parameters applied now to both datasets are summarized in Table 2.

The importance of static corrections at the Ketzin site was clear during the processing of the baseline data. Initially, the repeat data were processed with the old (baseline) static corrections and the resulting stacked seismic cube suffered from two obvious problems: (1) – some reflecting horizons were not as coherent as in the baseline cube; (2) – a cross-correlation time-shift of the repeat cube relative to the baseline showed a clear variation over the area and

had a noticeable NW-SE trend. This was an indication that the velocities in the subsurface were not the same as in 2005. Therefore, a new analysis of the first breaks, reconstruction of the near-surface low velocity zone and calculation of new refraction static corrections was necessary to accommodate these changes. Refraction statics for the repeat dataset were calculated with the same two-layer starting model, but with the new first breaks, re-picked in the repeat data in the 300-500 m offset interval.

Comparison of the baseline first arrivals with the new ones showed that the largest negative differences (2009 minus 2005) were observed in the NW, indicating that the arrival times were later and the subsurface velocities were slower during the 2005 acquisition relative to the 2009 acquisition. The largest positive values were in the SW, suggesting that the conditions were the opposite there with the subsurface velocities being slower during the 2009 repeat acquisition. The average first arrivals difference pattern shows the same regional NW-SE trend as the cross-correlation time shifts between the stacked seismic cubes, which were processed with the same original static corrections. This similarity is a strong indication that the main time shift difference between the datasets is concentrated in the shallow near-surface zone, since it is mainly the velocities in this zone that are influencing the first arrival times.

The differences in the refraction statics between the repeat and the baseline surveys are mainly in the order of -10 to 10 ms for receiver and source stations and in the order of -20 to 25 ms for total trace refraction statics. A predominance of positive differences (414542 versus 245582 traces) suggests that the data from 2009 were acquired with a thicker (or slower) low velocity zone and, therefore, should be generally shifted upward more during processing. New surface-consistent residual reflection statics were calculated after application of the new refraction statics and NMO corrections. The same velocity field from the original baseline processing was used for NMO corrections and for post-stack time migration of the repeat

data. The same pre-stack zero-phasing filter (step 14) obtained from the baseline data during the original processing was applied to the repeat data.

The post-stack processing, cross-calibration and analysis of the seismic volumes after step 24 (Table 2) was carried out using the interpretational software package *Pro4D*. The cross-calibration of the two stacked seismic cubes included cross-correlation, phase and time shifting, phase and frequency shaping by filtering, cross-normalization and time-variant shifting. The quality of the seismic match has been estimated from the normalized RMS error (NRMS) between the two volumes (Fig. 5). The NRMS measure compares seismic amplitudes of specified traces and is sensitive to static shifts, amplitude and phase differences. The NRMS values can range from 0% for identical traces (volumes) to 200% if one trace contains only zeroes or both traces (volumes) anti-correlate (Kragh and Christie 2001). The map of the NRMS values for the cross-calibrated seismic sub-volumes in the time interval of 100-700 ms (Fig. 5) shows quite good repeatability for most of the repeat 3D area (with a NRMS error in the order of 15-25%). The larger discrepancies at the margins of the surveyed area are due to the low fold and low signal amplitudes there. There are two localized areas, closer to the centre of the mini-3D survey, with higher (over 40%) NRMS anomalies, which highlight the time-lapse changes. The main southern anomaly is in the vicinity of the injection borehole and extends towards the north; the smaller second anomaly is located further to the northwest from the first one.

Table 2. Processing steps applied to the mini-3D data set compared with the original flow.

Step	Original parameters	New parameters
1	Read raw SEGD data	

2	Vertical diversity stack	
3	Bulk static shift to compensate for source delay: 6 ms	
4	Extract and apply geometry	
5	Trace edit and polarity reversal	
6	Pick first breaks: offset range 300–500 m	
7	Remove 50-Hz noise on selected receiver locations	
8	Spherical divergence correction: v^2t	
9	Band-pass filter: Butterworth 7–14–150–250 Hz	Bandpass filter: Butterworth 7-14-120-200 Hz
10	Surface consistent deconvolution: filter 120 ms, gap 16 ms, white noise 0.1%	
11	Ground roll mute	
12	Spectral equalization 20–40–90–120 Hz	Spectral equalization 20-35-80-110 Hz
13	Band-pass filter: 0–300 ms: 15–30–85–125 Hz 350–570 ms: 14–28–80–120 Hz 620–1000 ms: 12–25–70–105 Hz	Band-pass filter: 0-300 ms: 15-30-75-115 Hz 350-570 ms: 14-28-70-110 Hz 620-1000 ms: 12-25-60-95 Hz
14	Zero-phase filter	
15	Refraction statics: datum 30 m, replacement velocity 1800 m /s, v0 1000 m/s	
16	Trace balance using data window	

17	Velocity analysis: every 20th CDP in the inline and crossline direction	
18	Residual statics	
19	Normal moveout correction: 50% stretch mute	
20	Stack	
21	Trace balance: 0–1000 ms	
22	FX-Decon: Inline and crossline directions	
23	Trace balance: 0–1000 ms	
24	Migration: 3D FD using smoothed stacking velocities	
25	Depth conversion: using smoothed stacking velocities	

The main anomaly in the vicinity of the injection borehole reflects changes in amplitudes and waveforms that are most likely due to the injected CO_2. Fig. 6 shows vertical sections along in-line 1165 (a) and cross-line 1100 (b) highlighting the difference between the cross-calibrated volumes in the altered areas. The strongest time-lapse anomaly can be observed between cross-lines 1085 and 1110 (Fig. 6a) and between in-lines 1155-1175 (Fig. 6b) centered at approximately 40 ms below the picked K2 reflection (shown as the red line). The smaller NRMS anomaly to the northwest appears mainly due to changes above the K2 reflection. These changes may be partly due changes in the remnant gas distribution in the Jurassic reservoir rocks at the top of the anticline that were used for natural gas storage prior to 2004 (Juhlin *et al.* 2007).

In order to image the lateral distribution of amplitude variations related to the injected CO_2, the following work flow was executed. The traveltimes to the K2 reflection, related to the c. 20 m thick anhydrite layer within the cap rock, were picked in both time migrated volumes. The amplitude values 42 ms below the K2 reflection peak (corresponding to the approximate depth level of the top Stuttgart formation) were normalized to the peak amplitude of the K2 reflection and the repeat amplitudes were then subtracted from the baseline amplitudes (Fig. 7, left panel). A positive anomaly with the maximum located very close to the surface projection of the injection borehole outlines the area of more negative amplitudes in the repeat survey along the Stuttgart reservoir and provides a qualitative idea on where the CO_2 has migrated within the reservoir. The irregular pattern of the observed anomaly suggests variable permeability and reflects the generally complex character of the reservoir within the Stuttgart Formation.

The traveltime difference map (Fig. 7, right panel) shows increased time delays due to reduced velocities in the gas-saturated reservoir between the K2 horizon and a picked reflection below the reservoir (about 160 ms below K2). These delays of up to 4-5 ms are concentrated mostly in the vicinity of the injection site with some patches present in the western part of the survey area as well. The time delay anomaly is not as sharp and does not fit with the contours of the amplitude anomaly in the left panel of Fig. 7. This divergence may be due to the different sensitivity of the traveltimes and seismic amplitudes to the presence of gas in saline water aquifers and because of the relatively small amount of CO_2 (c. 22-25 kilotons) that had been injected up to the time of the repeat survey in 2009. Pressure differences in the reservoir may also influence the distribution of the anomalies.

The CO_2 induced amplitude anomaly extends in the repeat seismic cube for some 350 m in the in-line direction (cross-lines 1085-1110), 250 m in the cross-line direction (in-lines 1155-

1175) and 20 ms in time (515-535 ms). A more detailed estimation of the amount of CO_2 producing this anomaly is presented later in this paper. There are no indications of CO_2 leakage from the reservoir level in the repeat data, since there are no other time-lapse anomalies observed above the K2 reflection in the vicinity of the injection site.

PETROPHYSICAL LABORATORY EXPERIMENTS

The knowledge on the behaviour of petrophysical properties is crucial for the interpretation of well-logging and geophysical field monitoring data. Consequently, the effect of CO_2 injection on the petrophysical parameters of the Ketzin reservoir was investigated at laboratory scale on cores from the new CO_2Sink well Ktzi 202. The experimental scheme comprised analysis of density and porosity as well as the measurement of electrical resistivity, ultrasonic P and S wave velocities and permeability at constant pressures and temperature, simulating the conditions of the Ketzin reservoir (p_{conf} =15 MPa, p_{pore} = 7.5 MPa, and T = 40°C).

The experiments were conducted in an internally heated oil pressure vessel (Kulenkampff and Spangenberg 2005) at fluid flow conditions over periods of 16 and 20 days, respectively. Confining and pore pressure were controlled with syringe pumps. Corresponding to the field experiment the injection of CO_2 was carried out in a supercritical state. For this reason, the whole pore pressure system (pumps, valves, capillaries) was embedded in a thermal insulation system and heated up to the experimental working temperature of 40°C.

Two reservoir sandstone samples from the new Ketzin well Ktzi 202/2007 were used. The moderately to weakly consolidated sample material has been vacuum sealed at the drilling site. In the lab, both sample cores which endured the preparation procedures, were stored in the original formation brine in order to avoid the precipitation of salt and the clogging of pore

space. The investigated samples were fine grained and moderately sorted. The mineral content was dominated by angular fragments of quartz and feldspar, which were often coated by iron oxides and embedded in a clay-rich matrix. Additionally, sample B2_3b was partially cemented by anhydrite and dolomite. The porosity was 28.07 % for sample B2-3b and 28.45 % for sample B3_1b. For further details see Förster *et al.* (2010).

The sample cores with a diameter of 47.6 mm and different lengths (B2-3b = 49.41 mm; B3-1b = 44.50 mm) were placed between end caps made of Hastelloy (C2000). Sample and end caps were jacketed with a perfluoralkoxy heat shrinkable tubing. The end caps contain the pore pressure port, ultrasonic P- and S- wave transducers and act as current electrodes in a four-point electrical resistivity test assembly. The potential electrodes are punctually attached to the sample surface and contacted through the jacket. Sketches of the experimental set-up are shown in Kummerow and Spangenberg (2005).

Fig. 8 and Fig. 9 show the results of two flow experiments conducted with different brine-CO_2 injection schemes. The brine saturation was obtained from the recorded resistivity data by applying Archie's 2nd equation: $\frac{\rho_t}{\rho_0} = I = S_W^{-n}$, where ρ_0 is the resistivity of the fully brine saturated sample and ρ_t the resistivity at partial saturation. The saturation exponent n = 1.62 was determined at ambient conditions from sample B2-3b. Due to the high clay content of the Ketzin reservoir it is considerably lower than the standard value n = 2 for sandstones.

For the first sample, pure CO_2 was injected in the completely brine saturated sample for 7 days followed by 3 days with a CO_2-brine flow. Subsequently, the sample was re-saturated with formation brine again. The P-wave velocity of the completely brine saturated sample was 3.20 km/s and decreased to 2.73 km/s at a maximum CO_2 saturation of 53 %. After re-

saturation with brine the initial velocity of the fully brine saturated sample of 3.20 km/s was reached again. In contrast, the S wave velocity is nearly unaffected by the change of the pore fluid, varying about a mean value of 1.42 km/s ± 0.015 km/s.

The switching over from brine to CO_2 flow in the first experiment resulted in abrupt changes of the physical properties. Hence, for the second sample, the formation brine was incrementally replaced by CO_2 by applying a 2-phase flow (Fig. 9a). Each level of the 2-phase stream was held constant for 24 h. This gave us the opportunity to measure physical properties at distinct levels of partial saturation. Finally, the sample was re-saturated with formation brine. The P-wave velocity of the completely brine saturated sample was 3.07 km/s and decreased to 2.44 km/s after the sample was flooded with the CO_2 – brine stream and pure CO_2. After about 24 hours of re-saturation with pure brine flow the initial P-wave velocity of 3.08 km/s was reached again. As observed for sample B2-3b, the S wave velocities did not depend on the fluid flow medium and gave a mean value of 1.34 km/s ± 0.012 km/s. For the adjusted flow rates we did not observe any clear "drying effect" of supercritical CO_2 and maximum CO_2 saturations of 53 % for sample B2-3b and 41 % for sample B3-1b were attained.

Based on the measured data, fluid substitution models for homogeneous (Gassmann) and patchy saturation models (Kazemeini *et al.* 2010) were calculated for sample B2-3b (Fig. 10). Gassmann's relation (Gassmann 1951) has been used for the modelling in the following form:

$$K_{sat} = K_{dry} + \frac{\left(1 - \frac{K_{dry}}{K_{matrix}}\right)^2}{\frac{\phi}{K_{fluid}} + \frac{(1-\phi)}{K_{matrix}} - \frac{K_{dry}}{K_{matrix}^2}} \quad (1)$$

where φ is the sample porosity and K_{matrix}, K_{dry}, *and* K_{fluid} are the bulk moduli of the matrix material, the dry rock and the pore fluid, respectively. K_{matrix} was calculated considering the mineralogical composition of the rock material (Förster *et al*. 2010). The modulus and the density of the brine (215g/l NaCl) has been calculated for in situ conditions based on the equations of Batzle and Wang (1992). The modulus and density of CO_2 have been taken from the NIST data base (see Table 3).

Table 3: Bulk moduli and densities used for modelling.

	K (Gpa)	ρ (kg/m^3)
Matrix	37.78	2670.89
Brine	3.63	1164.59
CO_2	0.01	231.53

The density of the composite fluid was calculated with

$$\rho_{fluid} = \rho_{brine} S_W + (1 - S_W)\rho_{CO_2} \quad (2)$$

and the density of the saturated rock by

$$\rho_{sat} = \rho_{fluid}\phi + (1 - \phi)\rho_{matrix} \quad (3)$$

For the patchy model the approach of Kazemeini *et al.* (2010) was used, which is based on works of Hill (1963) and Berryman and Milton (1991):

$$K_{patchy} = \left[\sum_{i=1}^{n} \frac{x_i}{\left(K_{sat\_i} + \frac{4}{3} G \right)} \right]^{-1} - \frac{4}{3} G \quad (4)$$

Where n is the number of patches with different fluid content, x_i is the volume fraction of the ith patch, K_{sat_i} is the bulk modulus of the rock completely saturated with the ith fluid, and G is the shear modulus of the rock.

For the fully brine saturated sample, the measured velocity is considerably below the model prediction (Fig. 10). This is probably due to the high clay content of the Ketzin reservoir of about 20%. Water-saturated clay containing rocks often show a "weakening" of the frame and shear moduli and, thus, an assumption of the fluid-substitution models is not fulfilled. For the decreasing water saturation, the measured velocities rather follow the trend of a patchy saturation model. We assume that the CO_2 transport through the sample occurs via a few very permeable flow path ways and large patches of the sample remain fully brine saturated. Thus, the abrupt rise of the brine saturation S_W as a consequence of a reduction of the flow rate (Fig. 8b and Fig. 9b) might indicate a redistribution of brine in the pore network. The maximum error in the saturation estimation is 5.4%. It brings the measured data even closer to the trend of the patchy model. However, the application of a calibration under ambient conditions for an experiment under simulated in situ pressure involves the uncertainty that the estimation error might increase, since the electrical properties depend to a certain degree on pressure. The uncertainty of this approach will further increase when fluid-rock interaction causes changes in the structure of the fluid rock interface and the pore microstructure (Kummerow and Spangenberg 2011).

PULSED NEUTRON-GAMMA LOGGING

For monitoring of in-situ saturation changes at borehole scale the pulsed neutron-gamma (PNG) logging technique was applied at Ketzin. It is widely used for cased-hole saturation monitoring in oil and gas applications, and has previously also been applied successfully in

the Frio CO_2 injection pilot project (Sakurai *et al.* 2005). For the purpose of this study average minimum and maximum saturation values have been determined from the acquired logs.

Using the PNG method, the macroscopic thermal capture cross-section Σ is radiometrically measured (e.g. Plasek *et al.* 1995). The formation capture cross section depends on the capture cross section and the volumetric fractions of the individual components of the rock matrix and the pore fluids. For the current application, with the pore space either filled by brine or CO_2, Σ can be calculated according to the following equation (e.g. Ellis and Singer 2007, p. 393):

$$\sum = (1-\phi)\sum_{ma} + \phi S_W \Sigma_W + \phi(1-S_W)\Sigma_g \quad (5)$$

Where ϕ is the formation porosity, *S* fluid saturation, and the subscripts *ma*, *W* and *g* correspond to the rock matrix, the pore fluid brine, and the CO_2, respectively.

Changes in fluid saturation can be determined from comparison of time-lapse measurements before and after the start of CO_2 injection. Changes in the volumetric content of CO_2, $\phi(1-S_W)$, which is equal to V_g in Equation 6, can be calculated according to:

$$V_g = \frac{\Sigma_{\log} - \Sigma_{base}}{\Sigma_W - \Sigma_g} \quad (6)$$

where the subscripts *log* and *base* refer to the repeat and baseline logging runs (e.g. Ellis and Singer 2007, p. 393).

At Ketzin, favorable conditions for application of the PNG method exist because of the high formation water salinity of 240000 ppm and the high formation porosity, as well as the high contrast in Σ between saline formation water and CO_2. For the formation brine and CO_2 Σ, values of 120 c.u. (Schlumberger 2009) and 0.03 c.u. were used. Time-lapse measurements have been performed at Ketzin using the Reservoir Saturation Tool (RST, Trademark of Schlumberger). Immediately before the start of CO_2 injection, a baseline log was acquired in June 2008, with the wells filled with formation brine. The first PNG repeat was run on July 21st (r1), six days after the arrival of CO_2 at the Ktzi 200 observation well. Subsequent repeat runs were performed in June 2009 (r2) and March 2010 (r3) after the wells had filled up with CO_2.

Due to the temporal offset between the acquisition of the PNG logs and the 3D seismic survey, the results of the r2 and r3 PNG logging runs were averaged for the purpose of this study. Saturation changes were mainly observed within a limited number of continuous intervals with a clear correlation to lithology, with the highest changes occurring within the porous and permeable sandstone intervals (Fig. 11). Based on the acquired PNG data, two different scenarios were considerd, a minimum and a maximum one. The maximum scenario was based on the Σ formation values displayed in Fig. 11, which were computed using standard environmental corrections. For the minimum scenario, an empirically derived correction was applied, because the changes observed between the baseline and repeat logging runs are influenced by the uncemented sections of the annuli above the reservoir intervals being filled with CO_2 during the r2 and r3 repeat runs. This effect was compensated for by adding 2.4 to 7 c.u. to the individual Σ formation curves, leading to a reduced gas saturation in comparison to the original data.

Finally a number of individual sections were defined for each well (see Fig. 11) for which average CO_2 saturation values were calculated for the minimum and maximum saturation scenarios. Table 4 contains the geometries (top and bottom depths, thickness) of the intervals displayed in Fig. 11, as well as arithmetic averages of porosity (data after Norden *et al*. 2010), and CO_2 volume and saturation values calculated from the logging data for the respective intervals. The effective gas volume and saturation values listed for the Ktzi 200 and Ktzi 201 wells were calculated as weighted arithmetic mean values over all intervals of the respective well.

Table 4: Parameters for calculation of average CO_2 saturations from results of PNG logging (see Fig. 11 and text for further details).

Well	Interval Nr.	Top	Bottom	Thickness	Phi	Vg min.	Vg max.	Sg min.	Sg max.
		(m)	(m)	(m)	(%)	(%)	(%)	(%)	(%)
201	1	633.75	642.09	8.34	23.5	14	19	61	82
	2	642.87	650.99	8.12	25.9	8	13	29	49
	3	657.89	661.85	3.96	26.3	0	5	0	20
	4	661.85	664.11	2.26	27.2	0	3	0	11
	Eff.					**11**	**13**	**45**	**51**
200	1	634.58	642.24	7.66	27.5	13	17	45	60
	2	643.66	649.49	5.83	29.6	0	4	0	14
	Eff.					**13**	**11**	**45**	**39**
202	**1**	**627.55**	**635.98**	**8.43**	**28.2**	**6**	**12**	**23**	**44**

VOLUMETRIC (MASS) ESTIMATION

Chadwick, Arts and Eiken (2005) showed that it is possible to quantify to a certain degree the amount of CO_2 injected into a saline aquifer using time-lapse seismic measurements. Such

quantification is important for the assessment of storage efficiency and for the demonstration that there is no detectable leakage out of the reservoir formation. Furthermore, if leakage of CO_2 into a shallow aquifer has been detected, an estimation of the leakage quantity is needed in order to optimize remediation. We estimate here the mass of injected CO_2 using (i) the time-lapse normalized reflection amplitude difference map at reservoir level (Fig. 7, left panel), (ii) petrophysical measurements of P-wave velocities on reservoir core samples partly saturated with CO_2 and partly saturated with formation brine (see the chapter "Petrophysical Laboratory Experiments"), (iii) CO_2 saturation values determined from the PNG measurements in the three Ketzin wells for the minimum and maximum CO_2 saturation scenarios (see the previous chapter), and (iv) the travel-time difference map (Fig. 7, right panel). This difference (ΔT, velocity push-down) is a measure of the change in travel-time between two reflections, one above and one below the reservoir.

The following relation is used to estimate the mass of CO_2 (*MCO2*) contained in the imaged volume:

$$MCO2=\sum_N \Phi * SCO2 * \rho * dx * dy * H \qquad (7)$$

where Φ is the porosity of the reservoir which we assume to be the same in all CDP bins (the average value of porosity is taken from Förster *et al.* (2010), see Table 5), *SCO2* is the CO_2 saturation in the reservoir taken from the PNG minimum and maximum gas saturation scenarios (see Table 5), ρ is the CO_2 density derived using the monitored pressure and temperature conditions in the reservoir, $dx*dy$ is the size of one CDP bin (see Table 1), N is the total number of CDPs, and H is the thickness of that part of the reservoir containing CO_2. Note that a direct estimation of the CO_2 saturation from the seismic observations is currently

not possible, therefore we use the independent observations of the measured saturation in the three wells at the Ketzin site by the PNG logging.

The thickness of the layer containing CO_2, H, is derived from the velocity push-down effect, ΔT, using the following relation:

$$H = \Delta T / 2 (1/V2 - 1/V1) \quad (8)$$

where $V1$ and $V2$ are the P-wave seismic velocities in that part of the reservoir containing CO_2 before and after injection, respectively.

We assign CO_2 saturation values to each CDP bin by using an empirical approach based on the following observations. The maximum values of the normalized time-lapse amplitude map for the top of the Stuttgart formation are observed close to the injection location. With increasing distance from the injection location, the time-lapse amplitude decreases until it reaches an almost constant noise level at (normalized) values between 0.0 and 0.4 (Fig. 7, left panel). Independent from the seismic data, the borehole PNG measurements indicate decreasing CO_2 saturation away from the injection well (Table 4, "Sg min" and "Sg max" for minimum and maximum gas saturation scenarios, respectively). Therefore, we can transform the normalized time-lapse amplitude map to saturation levels using the saturation observations in the wells for calibration. Saturation values are assigned to the CDP locations according to Table 5.

Table 5: Parameters used for minimum (I) and maximum (II) CO_2 mass estimations according to minimum and maximum gas saturation scenarios from the chapter "Pulsed Neutron-Gamma (PNG) Logging".

Amplitude difference	CO_2 saturation (%)		P-wave velocity in the rock containing CO_2 (m/s)		P-wave velocity in 100% brine saturated rock (m/s)	CO_2 density in reservoir (kg/m³)
	I	II	I	II		
0.5-0.7	23	44	2900	2570	3135	266.62
0.7-0.9	45	39	2570	2580		
0.9-1.0	45	51	2570	2570		

P-wave velocities for the different CO_2 saturation values were estimated based on the petrophysical measurements described in the section "Petrophysical Laboratory Experiments". We used the average value of the P-wave velocities in the rock samples saturated with 100% brine (Table 5) for our estimate of the pre-injection velocity. For the CO_2 saturation levels of 23% and 39%, we linearly interpolated our measurements to obtain corresponding P-wave velocities (see Table 5). In addition, the velocities with the greatest obtained CO_2 saturation for every core sample were used for the 44%, 45% and 51% CO_2 saturation levels based on that the patchy saturation model appears to be valid for the Stuttgart Formation reservoir rocks (Fig. 10). These CO_2 saturation levels are also consistent with those observed from the PNG measurements (see Table 5). These velocities were used to calculate the CO_2 filled reservoir thickness with Equation (8). This calculation was done initially for

those CDPs where the normalized time-lapse amplitude difference exceeded 0.5 (Fig.7, left panel, see Table 5).

CO_2 mass calculations for the minimum and maximum CO_2 saturation values (Table 4) were made for every CDP bin and then the mass summed for all bins above the cutoff limit to give the total observed CO_2 mass (Fig. 12). The estimated total mass of the CO_2 for the minimum CO_2 saturation scenario (Fig. 12a) is about 20.5 kilotons. This value is about 7% less than the actual minimum quantity of the injected CO_2 to the time of the repeat survey (22.1 kilotons). The estimated total mass of the CO_2 for the maximum CO_2 saturation scenario (Fig. 12b) is about 23 kilotons. This value is about 5% below the actual maximum quantity of the injected CO_2 to the time of the repeat survey (24.2 kilotons).

DISCUSSION

Evaluation of the 3D time-lapse seismic measurements at the Ketzin CO_2 storage site shows a pronounced amplitude anomaly at the top of the storage reservoir, the Stuttgart Formation. The location of the amplitude anomaly (Fig. 7, left panel) is associated with the low fold area of the two surveys (Fig. 4), suggesting that the anomaly could be an acquisition artefact rather than a signature of the CO_2. However, the maximum change in amplitude is close to the amplitude of the K2 reflection and the anomaly is nearly centered on the injection well. In addition, since the K2 reflection corresponds to a positive impedance contrast, the positive nature of the amplitude difference anomaly indicates that it is due to a decrease in the impedance along the top of the Stuttgart Formation at the time of the repeat survey. This is also the expected response to the CO_2 injection, based on petrophysical measurements and modeling (this paper; Kazemeini *et al*. 2010). Therefore, we interpret the anomaly to be caused by partial CO_2 saturation and not an acquisition artefact.

The volumetric estimation, based on the seismic data in combination with core analyses and well logging, still contains some uncertainties for several reasons. First, sound waves may have a frequency dependent propagation velocity (e.g. White, 1975; Müller *et al.* 2010) so that the higher the frequency the higher the speed. At Ketzin, the average velocity from ultra-sonic laboratory experiments with 100% formation brine saturation (three measurements on two samples) is 3135 m/s, while on the logging data the average P-wave velocity is 3012 m/s in the reservoir sands. This velocity is close to what is observed on crosshole seismic data between the two observation wells. Although velocity dispersion is probably present in the Ketzin reservoir rocks, we do not consider it to be large enough that it could affect the mass of CO_2 in our estimation using the laboratory experiments. In addition, since we use the difference in velocity ($1/V1$-$1/V2$ in equation (8)) between brine saturated samples and those containing CO_2, the potential error made using the petrophysical results is reduced even more. Secondly, there are only a small number of direct petrophysical observations, providing a weak statistical basis for the determination of seismic velocities based on CO_2 saturation. An average P-wave velocity of 3012 m/s is observed at reservoir depths from the three Ketzin well sonic logs which, as discussed above, is somewhat lower than the brine saturated lab velocity, but close to the cross-hole velocity. We have assumed that the petrophysical experiments were carried out on samples that are representative for the average properties of the reservoir in the area close to the wells. Thirdly, the time difference velocity pushdown is not mapped very accurately (Fig. 7: right panel) as evidenced by large areas having similar differences as those in the vicinity of the injection well. Only to the east of the injection well there is a clear time difference anomaly of 5-6 ms. The rest of the time differences within the amplitude anomaly are near the noise level of 1-2 ms. A change of 1 ms in the time difference significantly affects the mass estimate for a given CDP bin. Thus, the application of a cutoff for the mass calculation based on the amplitude change map is crucial.

In order to check how changes in the lower amplitude limit influence the volumetric estimation, we assumed that CDP bins with amplitude difference values of 0.45-0.5 also contain injected CO_2. The minimum CO_2 mass value then becomes about 22.3 kilotons in this case. It is about 9% more than that of using amplitude difference values greater than 0.5 only. The maximum CO_2 mass value reached about 25.3 kilotons in this case. It is about 10% more than that of the amplitude difference using values greater than 0.5 only. If we instead assume that injected CO_2 is only contained in the CDP bins with amplitude difference values greater than 0.55 then the minimum CO_2 mass value is about 19.0 kilotons in this case. This is about 7% less than that using amplitude difference values greater than 0.5. The corresponding maximum CO_2 mass value is about 21.3 kilotons for the 0.55 cutoff which is about 7% less than that using amplitude difference values greater than 0.5 (see Fig.13).

CONCLUSIONS

We present here results of processing and interpretation of the first 3D repeat seismic survey for monitoring CO_2 storage at Ketzin. The repeat measurements are characterized by generally good repeatability, as shown in the NRMS map (Fig. 5). Results of processing, including equalization of the data sets and cross correlation, indicate that the CO_2 injected at the Ketzin site can be monitored. The size of the anomaly due to the CO_2 visible in the data is about 250 m in the S-N direction and about 350 m in the W-E direction. Petrophysical investigations on two core samples have been compared with Gassmann's theory of effective properties and patchy saturation models. Based on these results and geophysical logging of in-situ saturation, we have performed a preliminary mass quantification of the injected CO_2 as imaged with the seismic measurements. The resulting mass values differ within 5-7% from the actual quantity of the injected CO_2 to the time of the repeat survey. However, the estimation still contains some uncertainties. If the largest differences in amplitude (red areas

in the map of the Fig. 7, left panel) are interpreted as being due to the largest volumes of CO_2, then it appears that there is a higher concentration of CO_2 up-dip from the injection well, as expected. However, there also appears to be an asymmetry in the CO_2 plume, with more of the amplitude anomaly being present towards the west. In addition, a significant amount of CO_2 appears to have migrated down-dip.

It is known both from surface exposures (Förster *et al*. 2006) and from drilling at the CO2SINK site (Prevedel *et al*. 2008) that the Stuttgart Formation is lithologically heterogeneous. Therefore, it is not surprising that the CO_2 response is not symmetrical. The inhomogeneous pattern of the observed anomaly suggests variable permeability and is indicative of the generally complex character of the reservoir within the Stuttgart Formation. In addition, there were indications in the baseline 3D data that the injection site is located in a higher porosity zone of the Stuttgart Formation (Kazemeini *et al*. 2009).

CO_2 injection at Ketzin is planned to continue until 2013, and the ongoing injection will be monitored by future geophysical surveys. This will enhance the seismic signature of the CO_2 reservoir and provide further constraints for a stable mapping of the reservoir heterogeneity.

ACKNOWLEDGEMENTS

We are grateful for the highly committed cooperation in the field work with Geophysik GGD Leipzig (staking and surveying, seismic source), GTPro (permitting) and Hans Palm (acquisition coordination) that allowed for high quality data to be acquired in spite of sometimes difficult weather conditions. The 2005 baseline survey was mainly funded by the European Union (project CO_2SINK, no. 502599), the 2009 repeat survey was funded by the Geotechnologien programme of the German Federal Ministry of Education and Research,

BMBF (project 3DRep1, AZ 03G0679A). GLOBE Claritas^{TM} under license from the Institute of Geological and Nuclear Sciences Limited, Lower Hutt, New Zealand was used to process the seismic data. Hampson and Russell (CGG Veritas) provided Pro4D for the time lapse analysis. We thank the reviewers for their constructive criticism that helped to improve this paper. This is Geotechnologien paper number GEOTECH-1687.

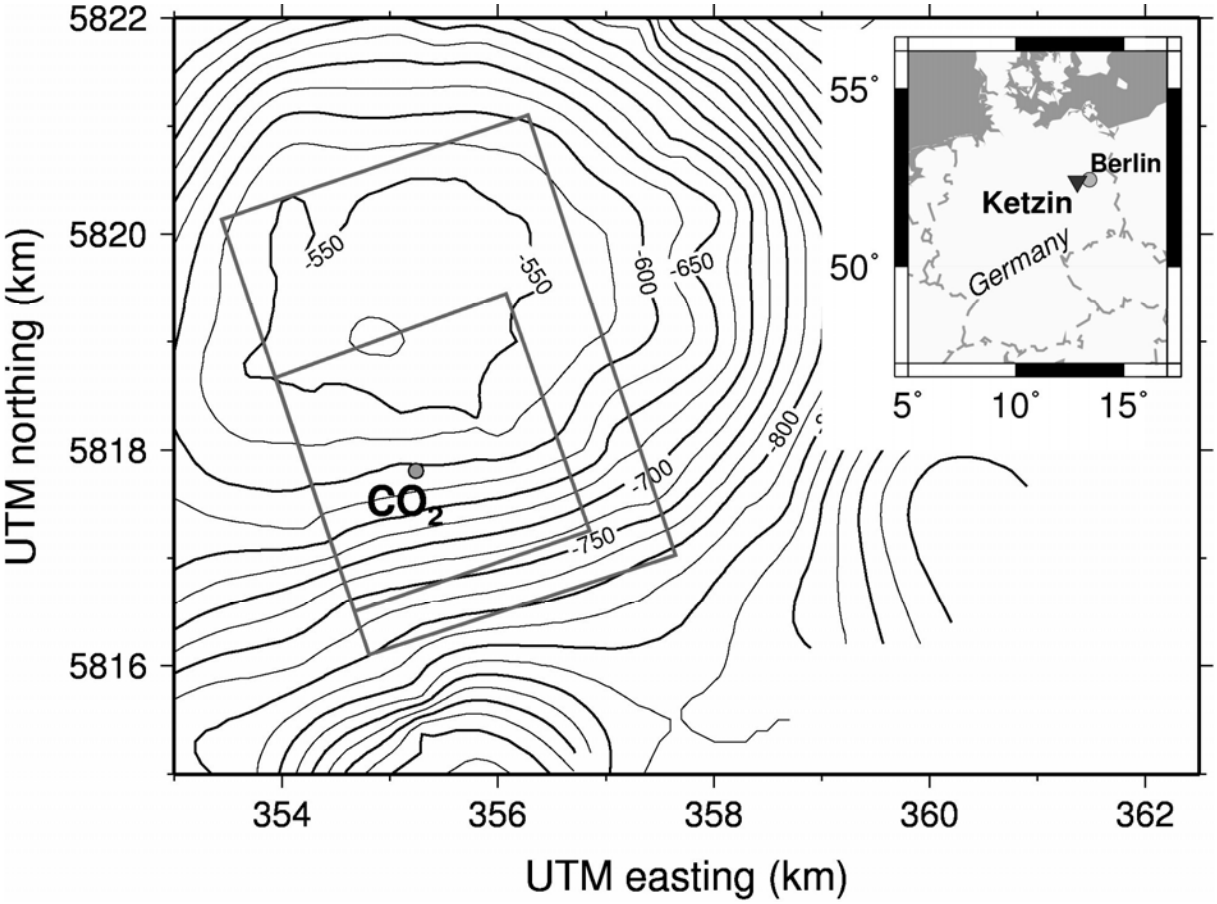

Figure 1: Depth contour lines of the top Stuttgart formation, showing the dome of the Ketzin anticline (Förster et al., 2009). The grey rectangles indicate the areas covered by the baseline and repeat 3D seismic surveys. The larger rectangle presents the 2005 baseline survey, the smaller rectangle presents the 2009 repeat survey concentrating on the area near the injection site ("CO_2") at the southern flank of the dome. The inset shows the location of the Ketzin site close to Berlin.

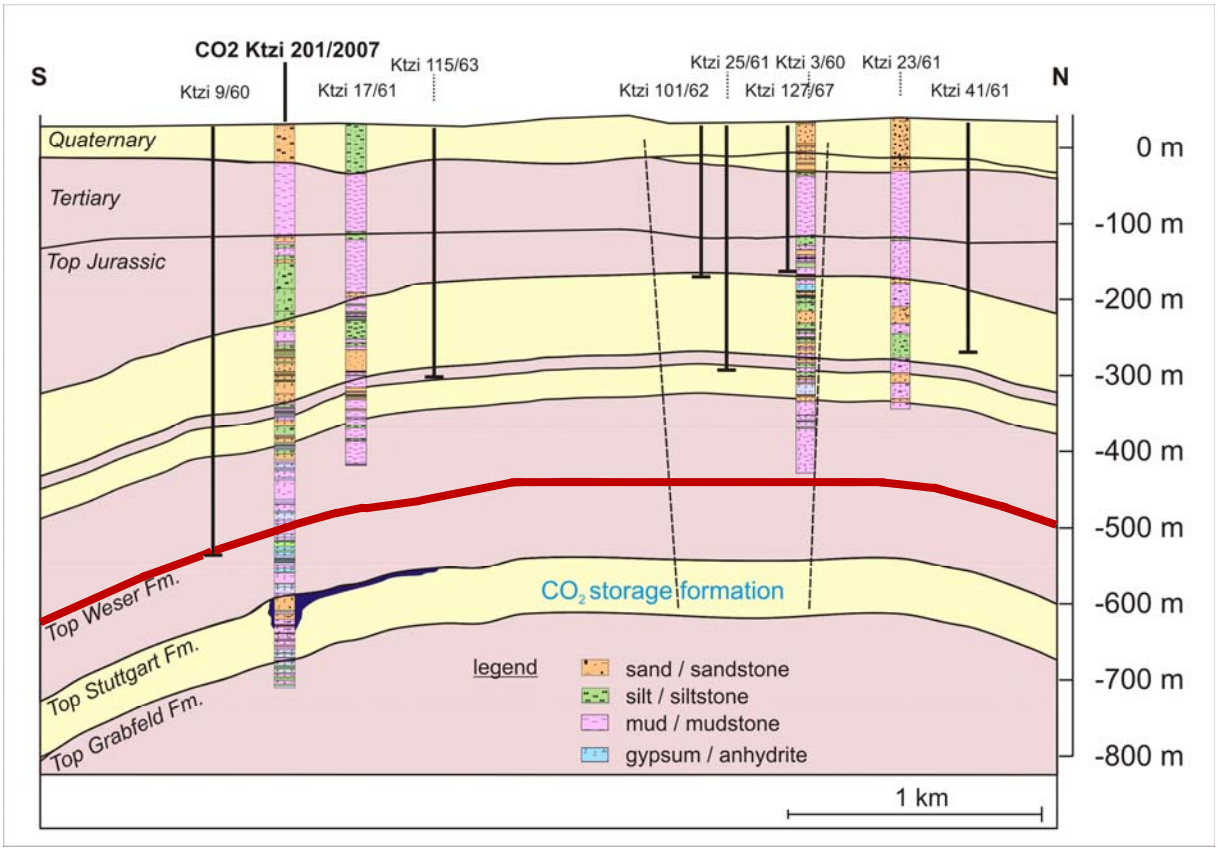

Figure 2: Simplified geological N-S cross-section of the Ketzin anticline (Förster et al., 2009). A schematic distribution of the injected CO_2 is indicated by the dark blue patch close to the Top Stuttgart Formation. K2 horizon is shown as a red layer.

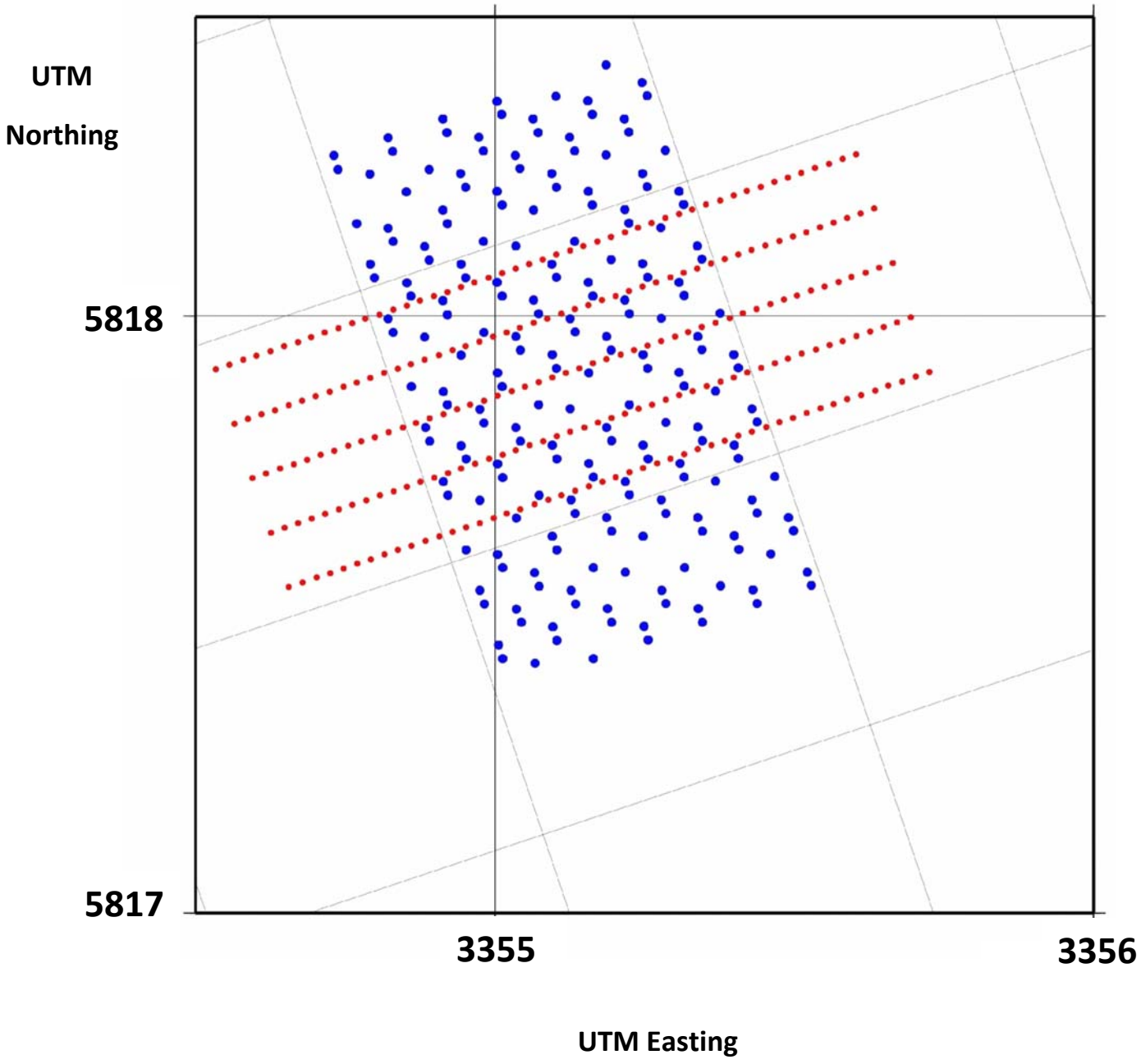

Figure 3: Sketch of a template shows locations of sources (red) and receivers (blue) (Juhlin *et al.* 2007). The repeat survey consists of 20 templates with neighbouring templates overlapping each other by 50%.

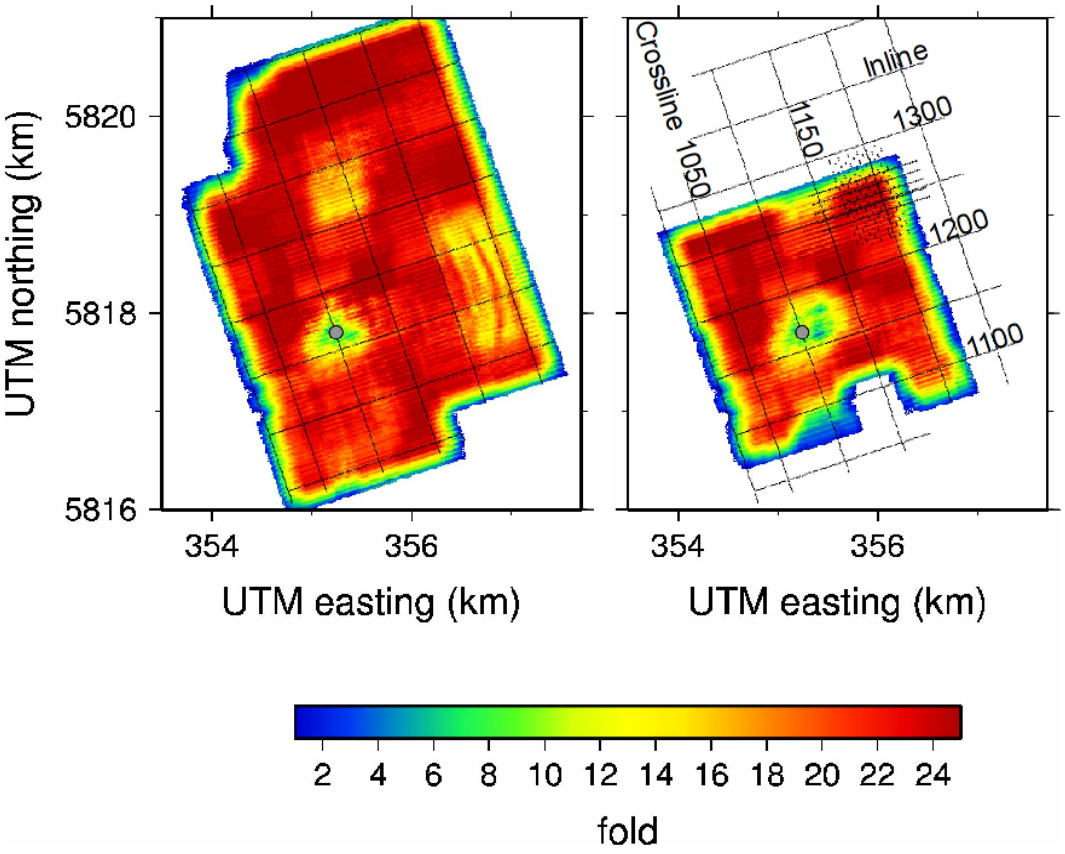

Figure 4: CDP fold of the 2005 baseline survey (left) and the 2009 repeat survey (right). The CO_2 injection well (CO2 Ktzi 201/2007) is marked by a grey dot. On the repeat survey (right panel), one template of shot and receiver lines is shown at the northern end of the survey. SW-NE lines are receiver points, NW-SE lines are shot points. In the repeat survey, the gap in fold map at the southern end of the area is due to bad weather conditions making some fields inaccessible for the source. Inline and crossline numbers are displayed for reference to stacked sections shown in later figures.

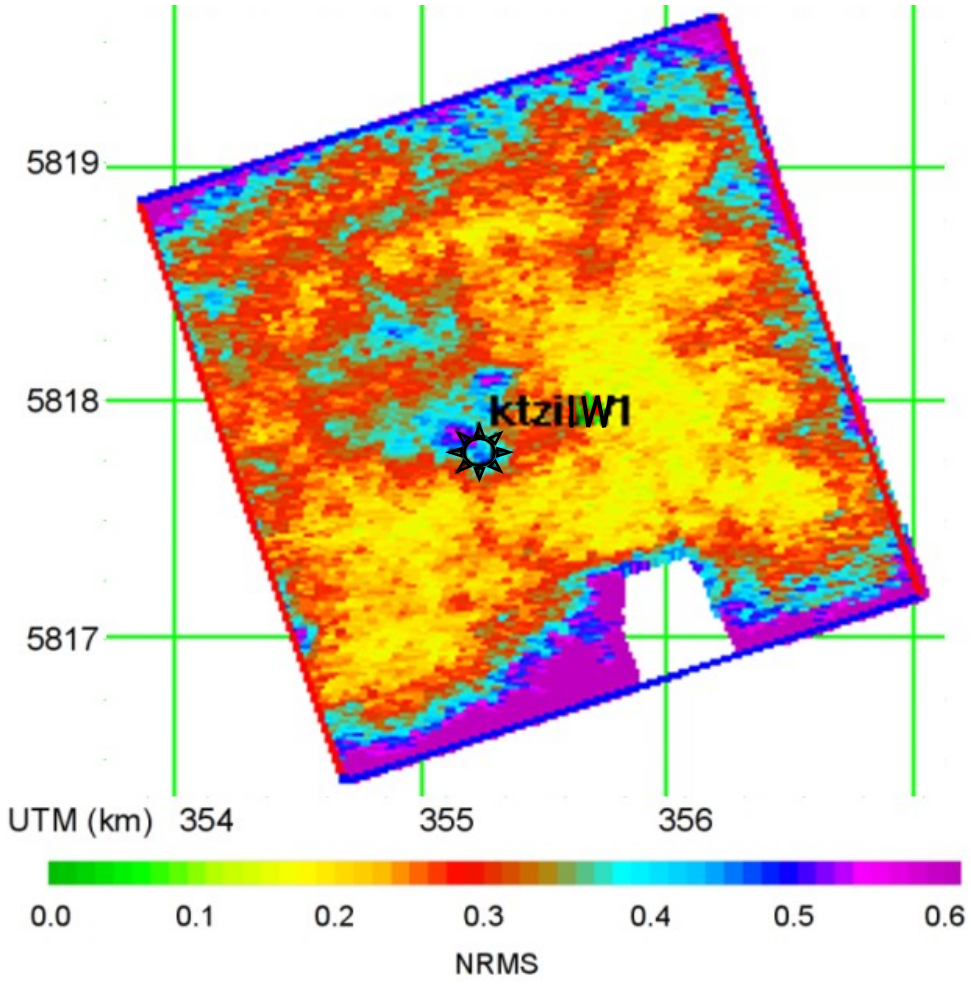

Figure 5: Map of the NRMS values for the cross-calibrated seismic sub-volumes in the time interval of 100-700 ms. The injection site is marked by a sun.

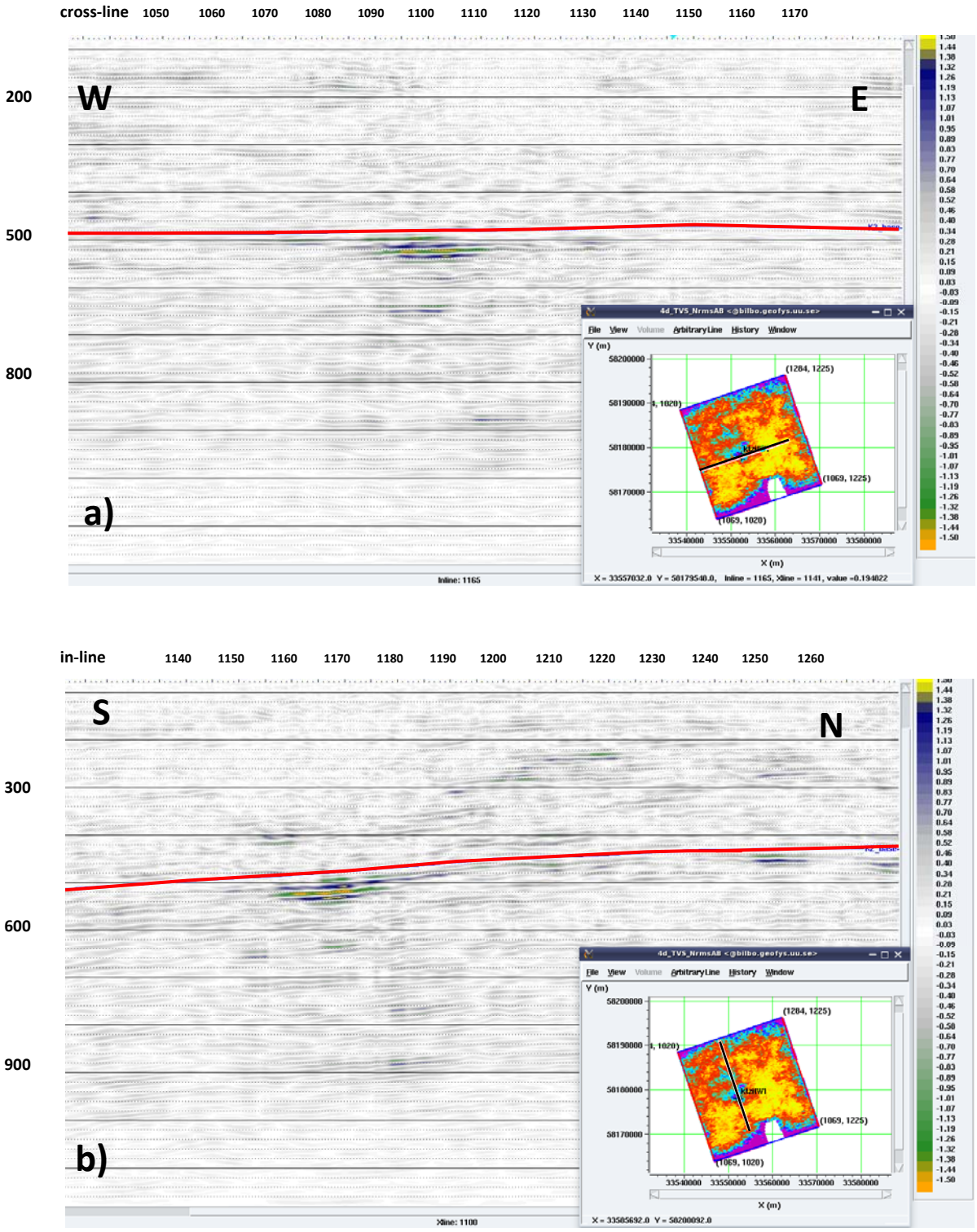

Figure 6: In-line 1165 (a) and cross-line 1100 (b) with the colours highlighting the difference between the cross-calibrated volumes. The vertical axes indicate time in milliseconds. The K2 reflection is shown as a red line in both sections. Black lines in the inset NRMS maps show locations of the sections.

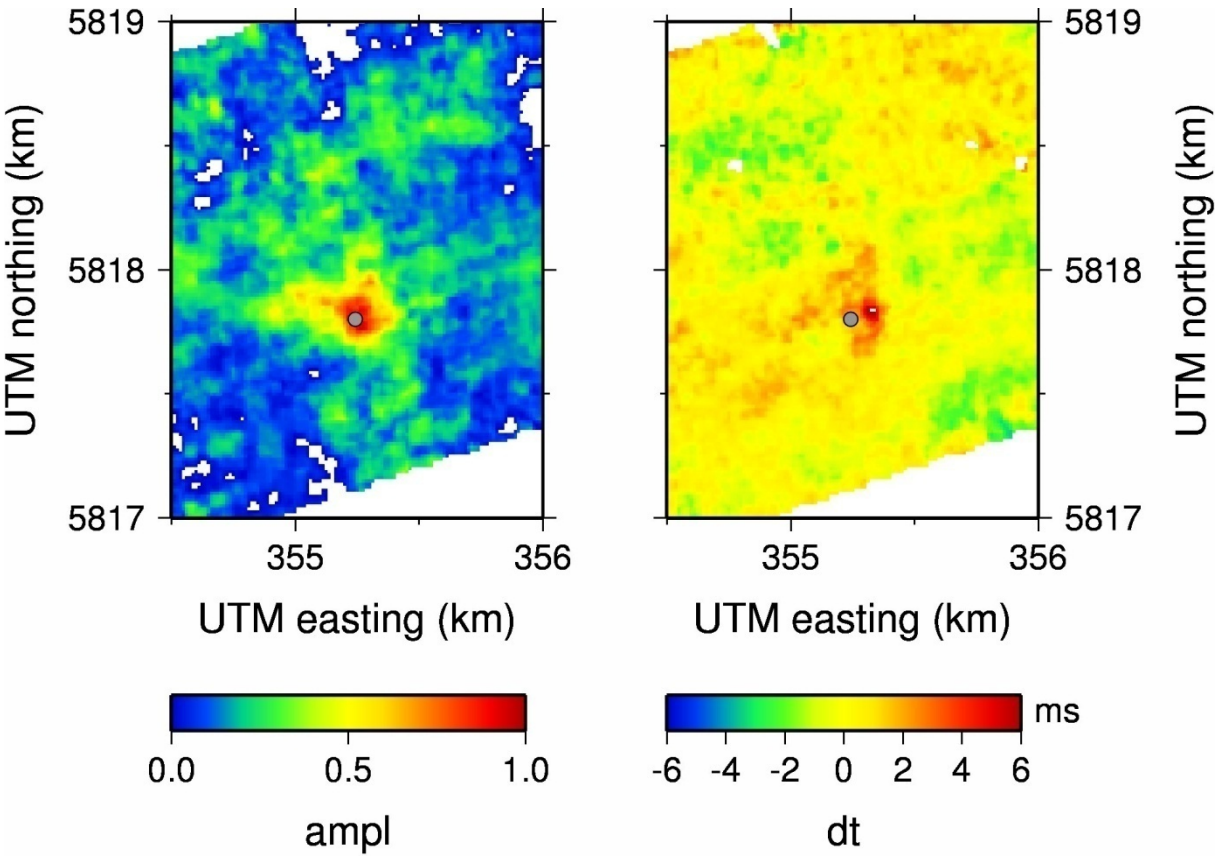

Figure 7: Left panel: Normalized time-lapse amplitude at 42 ms below the K2 horizon. Right panel: Time shift of a reflection below the reservoir caused by a velocity pull-down effect due to partial CO_2 saturation in the Stuttgart formation or pressure increases.

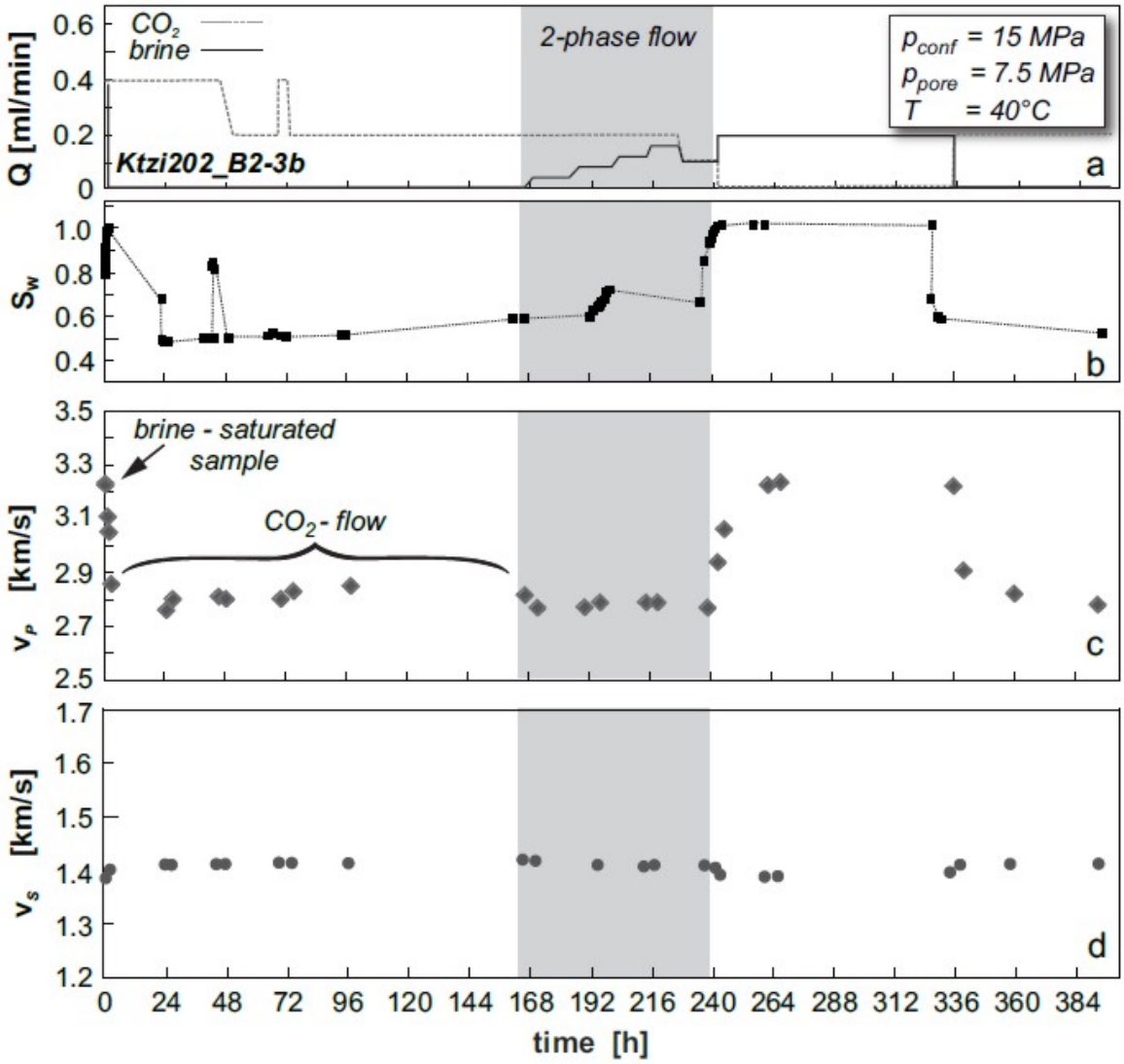

Figure 8: (a) Injection scheme of the flow experiment on sample Ktzi202_B2-3b plotted over the experimental run-time. (b) The brine saturation (S_W) was obtained from the measured electrical resistivity data. The uncertainty is 5%. (c and d) P and S wave velocities of the sample were measured at simulated in-situ conditions (p_{conf} = 15 MPa, p_{pore} = 7.5 MPa, T = 40°C). The error on ultrasonic velocities is ± 0.2%.

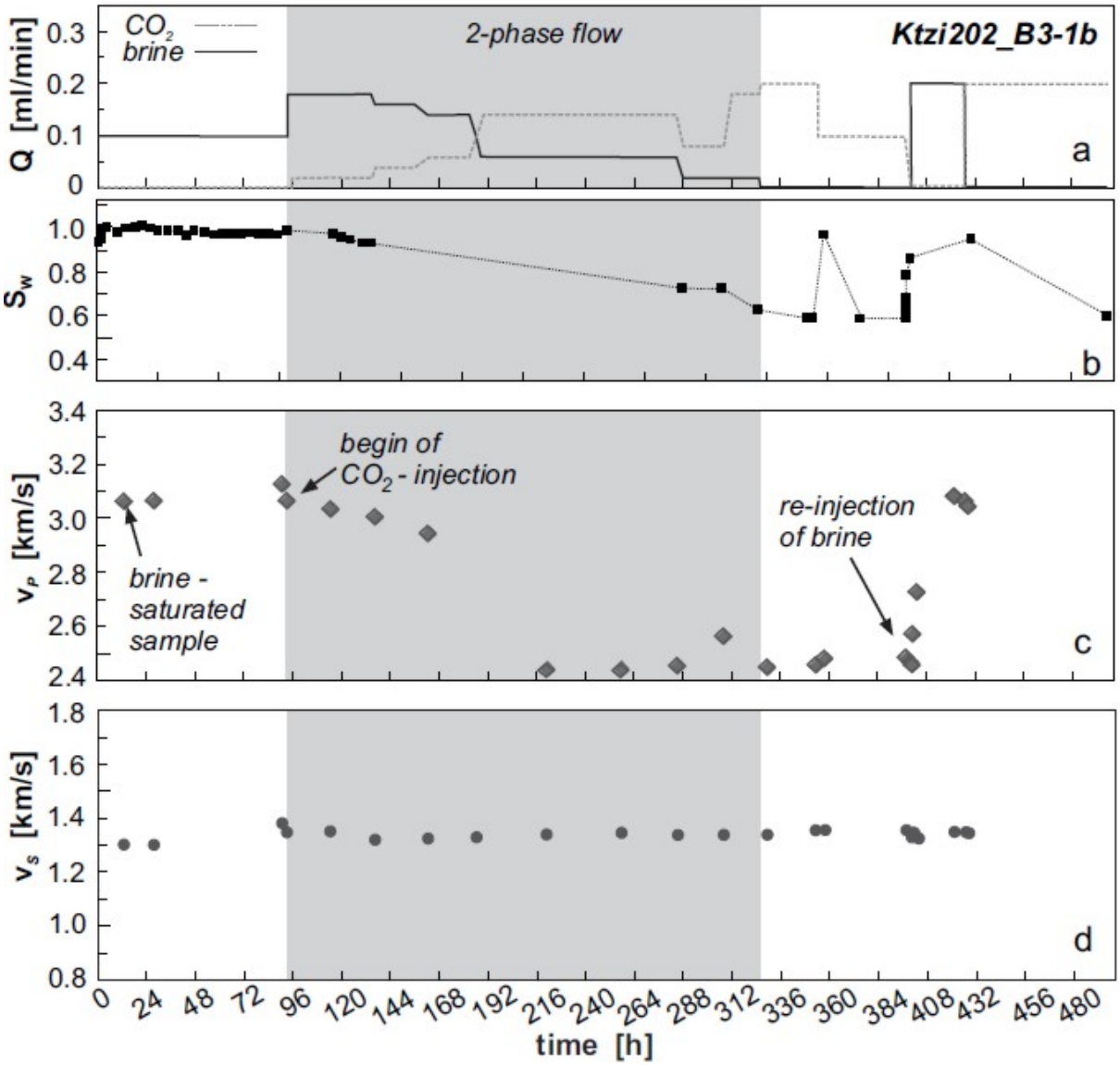

Figure 9: Injection scheme (a), brine saturation (S_W) (b) and P and S wave velocities (c and d) of sample Ktzi202_B3-1b as function of the experimental run-time. The flow experiment was conducted at simulated in-situ conditions (p_{conf} = 15 MPa, p_{pore} = 7.5 MPa, T = 40°C). The uncertainty of S_W determined from electrical resistivity measurements is 5%. The error on ultrasonic velocities is ± 0.2%.

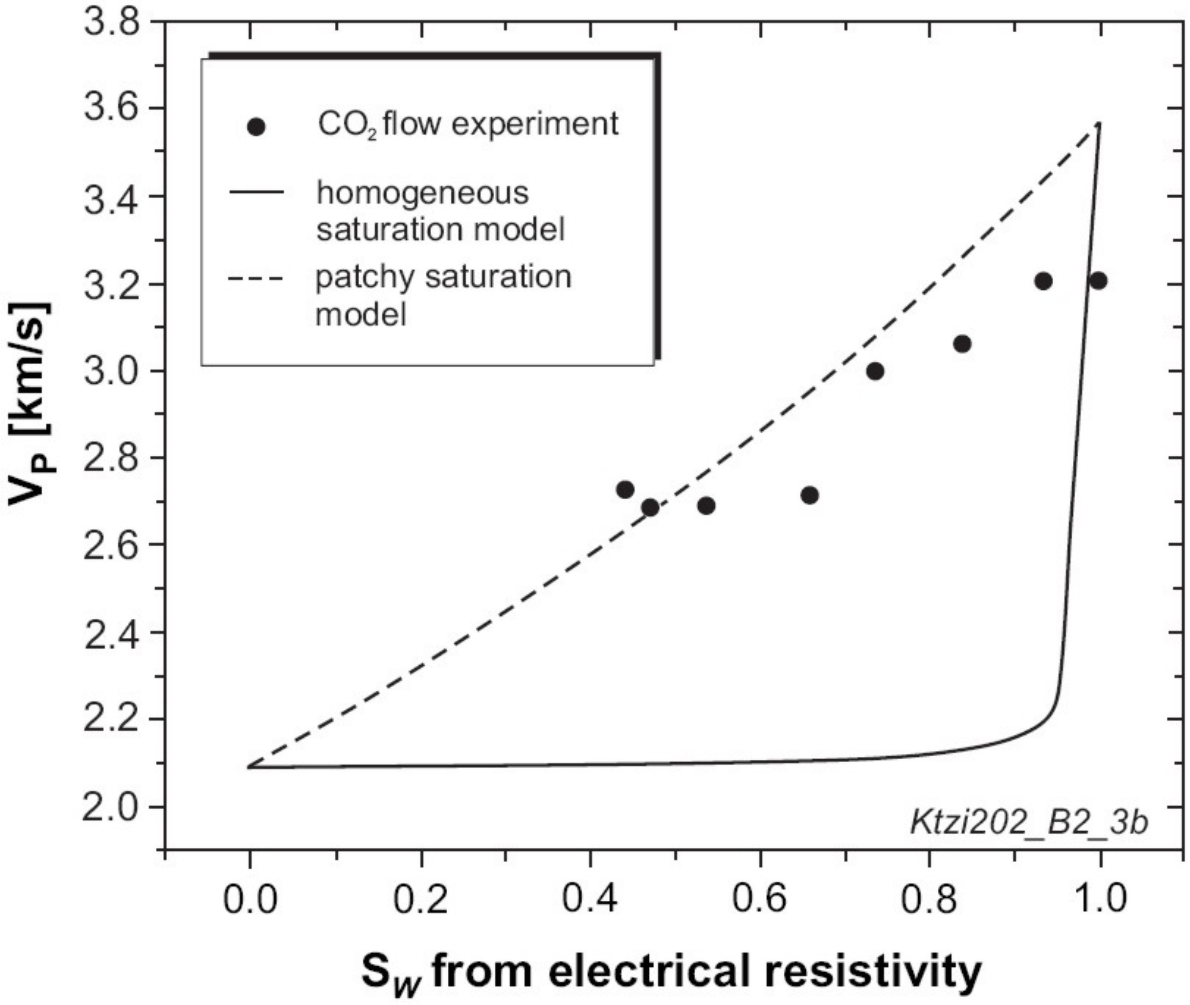

Figure 10: Results of fluid substitution modelling for sample Ktzi202_B2-3b.

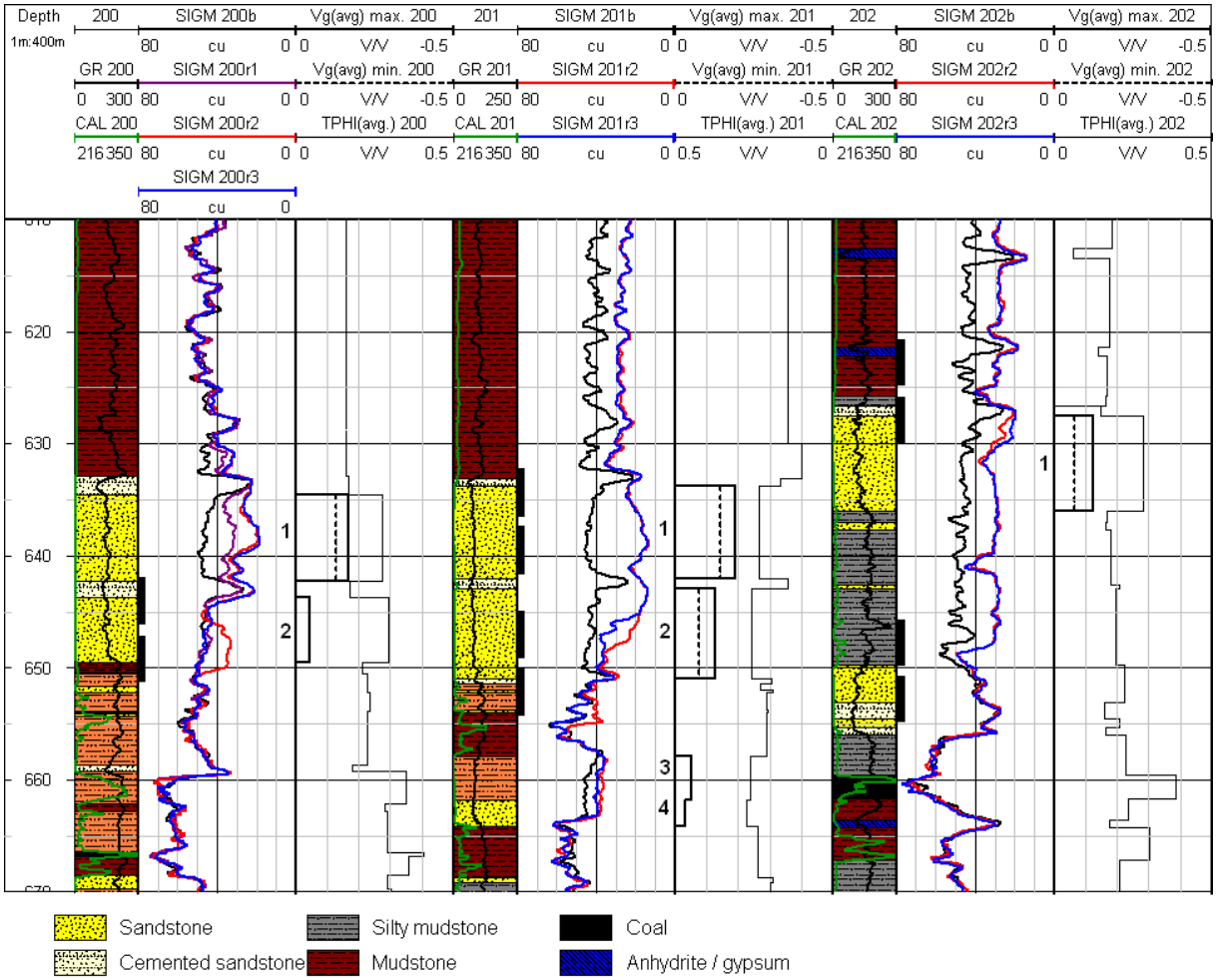

Figure 11: Measured PNG Σ formation (SIGM) log curves of the baseline (b) and repeat (r1, r2, r3) logging runs, and calculated average relative gas volumes (Vg(avg)) for the minimum (min.) and maximum (max.) estimations. TPHI(avg.): Average total porosity (modified after Norden *et al.*, 2010). Lithology after Förster *et al.*, 2010. The positions of the filter sections in the casing are indicated by black bars. Numbers of depth intervals for calculation of average CO_2 volumes and saturations (see Table 4) are indicated with bold numerals.

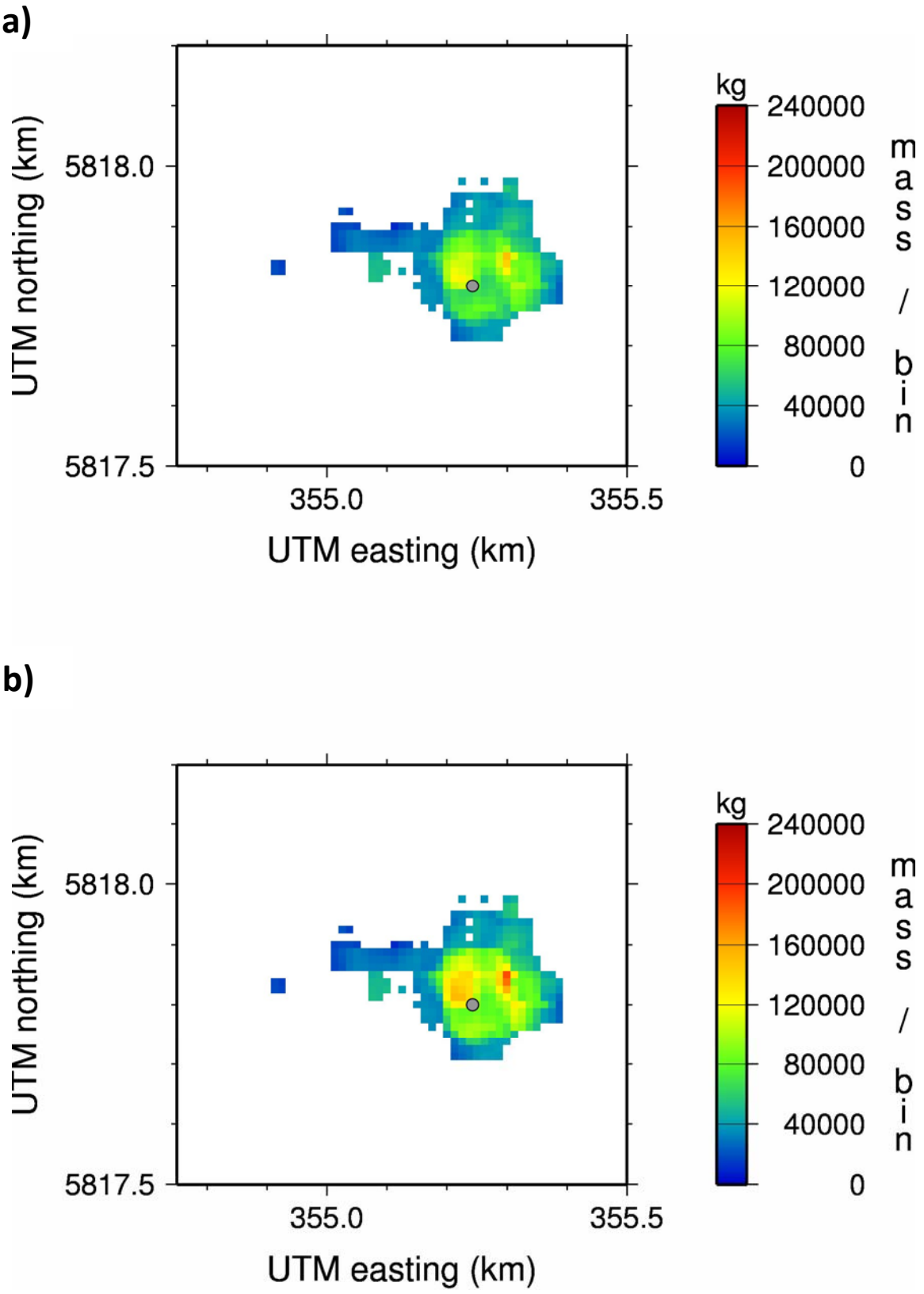

Figure 12: CO_2 mass maps for minimum (a) and maximum (b) CO_2 saturation scenarios calculated for every CDP bin where the amplitude difference value is greater than 0.5.

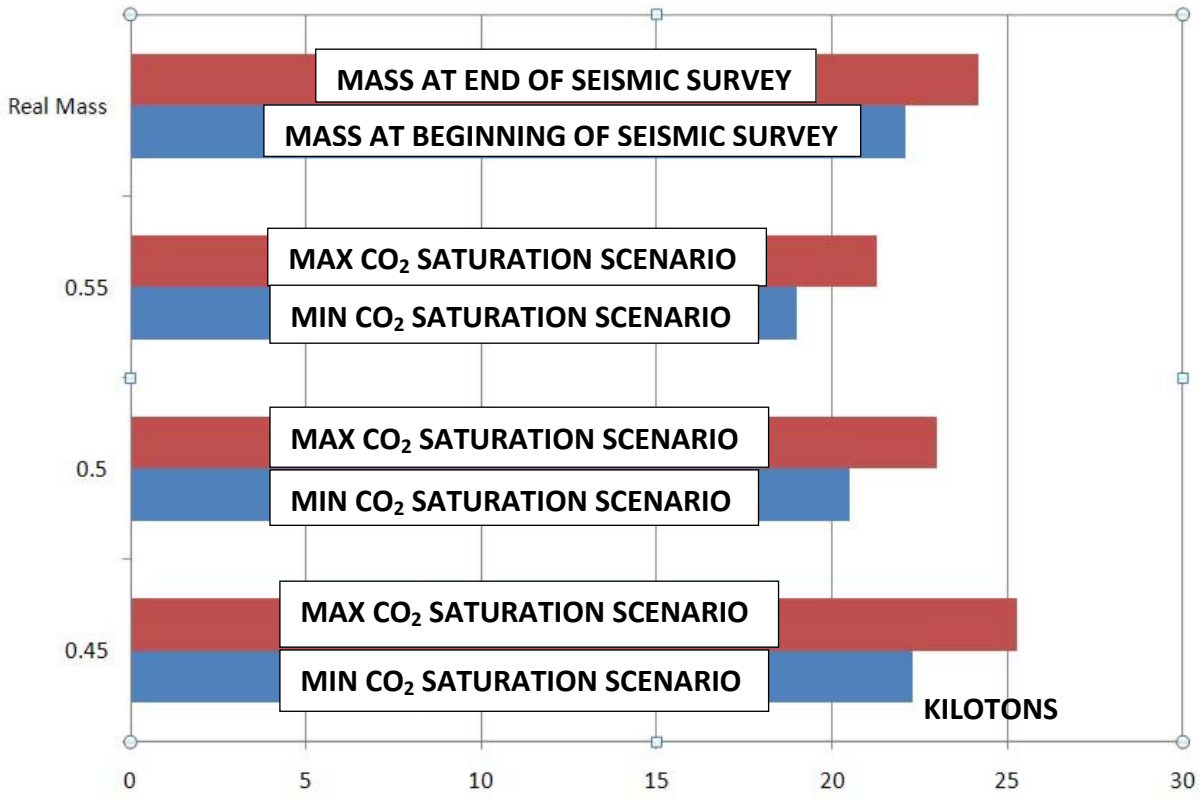

Figure 13: Diagram illustrating how changes in the cutoff influence the volumetric estimation. The vertical axis represents the following scenarios: "Real Mass" – mass of injected CO_2 to the time of the 3D repeat survey, "0.55-1", "0.5-1" and "0.55-1" – estimated CO_2 mass, if all the CDP-bins with amplitude difference values from 0.55 to 1.0, from 0.5 to 1.0 and from 0.55 to 1.0 respectively would contain CO_2.

REFERENCES

Arts R., Eiken O., Chadwick A., Zweigel P., van der Meer L. and Zinszner B. 2004. Monitoring of CO2 injected at Sleipner using time lapse seismic data. *Energy* **29**, 1383–1392.

Bachu S. 2003. Screening and ranking of sedimentary basins for sequestration of CO_2 in geological media in response to climate change. *Environmental Geology* **44**, 277–289.

Batzle M. and Wang Z. 1992. Seismic properties of pore fluids. *Geophysics* **57**, 11, 1396-1408.

Bergmann P., Yang C, Luth S., Juhlin C. and Cosma C. 2011. Time-lapse processing of 2D seismic profiles with testing of static correction methods at the CO2 injection site Ketzin (Germany). *J. Applied Geophysics* **75**, 124–139.

Berryman J.G. and Milton G.W. 1991. Exact results for generalized Gassmann's equation in composite porous media with two constituents. *Geophysics* **56**, 1950–1960.

Chadwick R.A, Arts R. and Eiken O. 2005. 4D seismic quantification of a CO2 plume at Sleipner, North Sea. In: *Petroleum Geology: North-West Europe and Global Perspectives* (ed. A.G. Dore and B.A. Vining), pp.1385-1399. The Geological Society, London. ISNB 1862391645.

Eiken O., Brevik I., Arts R., Lindeberg E. and Fagervik K. 2000. Seismic monitoring of CO_2 injected into a marine aquifer. SEG 2000 Expanded Abstracts, Calgary.

Ellis D.V. and Singer J.M. 2007. Well Logging for Earth Scientists. Springer. ISBN 1402037384.

Förster A., Norden B., Zinck-Jørgensen K., Frykman P., Kulenkampff J., Spangenberg E., Erzinger J., Zimmer M., Kopp J., Borm G., Juhlin C., Cosma C. and Hurter. S. 2006. Baseline characterization of CO2SINK geological storage site at Ketzin, Germany. *Environmental Geosciences* **13**, 145-160.

Förster A., Giese R., Juhlin C., Norden B., Springer N. and CO_2SINK Group. 2009. The Geology of the CO_2SINK Site: From Regional Scale to Laboratory Scale. *Energy Procedia* **1**, Issue 1, 2087-2094.

Förster A., Schöner R., Förster H.-J., Norden B., Blaschke A.-W., Luckert J., Beutler G., Gaupp R. and Rhede D. 2010. Reservoir characterization of a CO_2 storage aquifer: the Upper Triassic Stuttgart Formation in the Northeast German Basin. *Marine and Petroleum Geology* **27**(10), 2156-2172.

Gassmann, F. 1951. Über die Elastizität poröser Medien. *Vierteljahrsschrift der Naturforschenden Gesellschaft in Zürich* **96**, 1-23.

Giese R., Henninges J., Lüth S., Morozova D., Schmidt-Hattenberger C., Würdemann H., Zimmer M., Cosma C., Juhlin C. and CO2SINK Group. 2009. Monitoring at the CO2SINK Site: A Concept Integrating Geophysics, Geochemistry and Microbiology. *Energy Procedia* **1**, Issue 1, February 2009, 2251-2259.

Gonzalez-Carballo A., Guyonnet P.-Y., Levallois B., Veillerette A. and Deboiasne R. 2006. 4D monitoring in Angola and its impact on reservoir understanding and economics. *The Leading Edge* **1,** September 2006, no. 9, 1150-1159.

Hill R. 1963. Elastic properties of reinforced solids: some theoretical principles. *J. Mech. Phys. Solids* **11**, 357–372.

IPCC. 2005. In: *IPCC Special Report on Carbon Dioxide Capture and Storage, Prepared by Working Group III of the Intergovernmental Panel on Climate Change* (ed. B. Metz, O. Davidson, H.C. de Coninck, M. Loos and L. Meyer). Cambridge University Press. ISNB 9291691186.

Juhlin C., Giese R., Zinck-Jørgensen K., Cosma C., Kazemeini H., Juhojuntti N., Lüth S., Norden B., and Förster A. 2007. 3D baseline seismics at Ketzin, Germany: The CO2SINK project. *Geophysics* **72**, 121–132.

Kazemeini H., Juhlin C., Zinck-Jørgensen K. and Norden B. 2009. Application of the continuous wavelet transform on seismic data for mapping of channel deposits and gas detection at the CO2SINK site, Ketzin, Germany. *Geophysical Prospecting* **57**, 111–123.

Kazemeini S.H., Juhlin C. and Fomel S. 2010. Monitoring CO2 response on surface seismic data; a rock physics and seismic modeling feasibility study at the CO2 sequestration site, Ketzin, Germany. *Journal of Applied Geophysics* **71**, 109-124.

Kikuta K., Hongo S., Tanase D. and Ohsumi T. 2004. Field test of CO_2 injection in Nagaoka, Japan. In: *Proceedings of the 7th International Conference on Greenhouse Gas Control*

Technologies (GHGT-7) Vancouver, Canada, September 5–9, 2004 (ed. M. Wilson, T. Morris, J. Gale and K. Thambimuthu), pp. 1367–1372. ISNB 008044704.

Kragh Ed. and Christie Ph. 2001. Seismic Repeatability, Normalized RMS and Predictability, SEG Expanded Abstracts 2001.

Kulenkampff J. and Spangenberg E. 2005. Physical properties of cores from the Mallik 5L-38 production research well under simulated in situ conditions using the Field Laboratory Experimental Core Analysis System (FLECAS). In: *Scientific Results from the Mallik 2002 Gas Hydrate Production Research Well Program, Mackenzie Delta, Northwest Territories, Canada* (ed. Dallimore, S. R. and Collett, T. S.). Geological Survey of Canada. CD-ROM.

Kummerow J. and Spangenberg E. 2011. Experimental evaluation of the impact of the interactions of CO_2-SO_2, brine, and reservoir rock on petrophysical properties: A case study from the Ketzin test site, Germany. *Geochem. Geophys. Geosyst.* **12**(5), 1-10.

Lumley D., Adams D., Meadows M., Cole S. and Ergas R. 2003. 4D seismic pressure-saturation inversion at Gullfaks Field, Norway. *First Break* **21**, 49-56.

Meadows M. 2008. Time-lapse seismic modeling and inversion of CO_2 saturation for storage and enhanced oil recovery. *The Leading Edge* **27**, 506–516.

Michael K., Allinson G., Golab A., Sharma S. and Shulakova V. 2010. Geological storage of CO2 in saline aquifers - A review of the experience from existing storage operations. *Energy Procedia* **1**, 1973-1980.

Müller T. M., Gurevich B. and Lebedev M. 2010. Seismic wave attenuation and dispersion resulting from wave-induced flow in porous rocks — A review. *Geophysics* **75**, A147–A164, DOI: 10.1190/1.3463417.

Norden B., Förster A., Vu-Hoang D., Marcelis F., Springer N. and Le Nir I. 2010. Lithological and Petrophysical Core-Log Interpretation in CO2SINK, the European CO2 Onshore Research Storage and Verification Project. *SPE Reservoir Evaluation & Engineering* **13**(2), 179-192.

Plasek R. E., Adolph R.A., Stoller C., Willis D.J., Bordon E.E. and M. Portal M.G. 1995. Improved pulsed neutron capture logging with slim carbon-oxygen tools: Methodology, SPE 30598. Paper presented at SPE Annual Technical Conference and Exhibition, Society of Petroleum Engineers, Inc., Dallas, Texas, 22-25 October.

Prevedel B., Wohlgemuth L., Henninges J., Krüger K., Norden B., Förster A. and the CO2SINK Drilling Group. 2008. The CO2SINK boreholes for geological storage testing. *Scientific Drilling* **6**, 32-37.

Ringrose P., Atbi M., Mason D., Espinassous M., Myhrer O., Iding M., Mathieson A. and Wright I. 2009. Plume Development Around Well KB-502 at the In Salah CO2 Storage Site. *First Break* **27**, 85-89.

Sakurai S., Ramakrishnan T.S., Boyd A., Mueller N. and Hovorka S. 2005. Monitoring saturation changes for CO2 sequestration: petrophysical support of the Frio brine pilot experiment. 46th Annual Logging Symposium Transactions, Society of Petrophysicists and Well Log Analysts, New Orleans, Louisiana.

Schilling F., Borm G., Würdemann H., Möller F., Kühn M. and CO_2SINK Group. 2009. Status Report on the First European on-shore CO_2 Storage Site at Ketzin (Germany). *Energy Procedia* **1**, 2029 - 2035.

Schlumberger. 2009. Log Interpretation Charts, Schlumberger, Texas.

White J. E. 1975. Computed seismic speeds and attenuation in rocks with partial gas saturation. *Geophysics* **40**, 224–232.

Würdemann H., Moeller F., Kühn M., Heidug W., Christensen N.P., Borm G., Schilling F.R. and the CO_2SINKGroup. 2010. CO_2SINK – From Site Characterisation and Risk Assessment to Monitoring and Verification: One Year of Operational Experience with the Field Laboratory for CO_2 Storage at Ketzin, Germany. *International Journal of Greenhouse Gas Control* **4,** 938-951.